A Noise-Aware Convolutional Neural Network for Noise Reduction and Resolution Enhancement in Chest X-Ray Images

Laxmibai
Department of Electronics and Communication Engineering, Sharnbasva University, Kalaburagi, India
laxmibairesearch@gmail.com (corresponding author)

Vinita Patil
Department of Electronics and Communication Engineering, Lingaraj Appa Engineering College, Bidar, India
vinita.pratapur@gmail.com

Received: 23 September 2025 | Revised: 17 December 2025 | Accepted: 24 December 2025

 DOI: https://doi.org/10.48084/etasr.15045

ABSTRACT

Low-resolution medical images, especially Chest X-Rays (CXRs), often suffer from noise and blurriness, hindering accurate diagnosis. This study introduces the Noise-Aware Convolutional Neural Network (NA-CNN) architecture to address this issue. The objective is to enhance image quality by eliminating noise and converting low-resolution images into high-resolution images. The methodology involves a Convolutional Neural Network (CNN)-based model integrated with sparse coding reconstruction, adaptive downsampling, and nonlinear mapping. Evaluations were conducted on a high-performance system using the COVID-19 Radiography dataset. The results demonstrated that NA-CNN consistently outperformed the existing CNN model, achieving higher Peak Signal-to-Noise-Ratio (PSNR) and Structural Similarity Index Measure (SSIM) values across various noise levels, indicating superior image quality and structural fidelity. The novelty of this work lies in its innovative architecture that combines a CNN with adaptive techniques, resulting in efficient and high-quality image enhancement. NA-CNN's robustness and efficiency make it a valuable tool for medical image processing, providing significant advancements over existing methods.

Keywords-low-resolution images; Noise-Aware Convolutional Neural Network (NA-CNN); sparse coding reconstruction; Chest X-Rays (CXRs); PSNR; SSIM

I. INTRODUCTION

The respiratory system is a vital component of the human body, responsible for supplying oxygen to the bloodstream and removing carbon dioxide, a by-product of metabolism. However, it is highly susceptible to a wide range of diseases arising from infections, chronic conditions, environmental factors, and genetic predispositions. Common respiratory diseases include asthma, Chronic Obstructive Pulmonary Disease (COPD), pneumonia, and lung cancer [1]. These conditions manifest through symptoms such as shortness of breath, coughing, wheezing, and chest pain, and significantly impair the quality of life. More recently, the COVID-19 pandemic, caused by the SARS-CoV-2 virus, has highlighted the global vulnerability of the respiratory system [2]. The virus's ability to cause severe lung inflammation and damage has resulted in substantial morbidity and mortality worldwide.

To improve early detection and diagnosis of such diseases, Artificial Intelligence (AI) has emerged as a powerful tool in medical imaging. In particular, Deep Learning (DL) and Machine Learning (ML) algorithms have shown considerable potential in analyzing Chest X-Ray (CXR) images [3]. These approaches can identify patterns and abnormalities that are indicative of respiratory conditions, often with performance comparable to, or even surpassing, that of human experts. While most existing research has emphasized disease classification using CXRs, an equally important yet often overlooked step is image preprocessing, especially noise removal [4-13]. For example, authors in [4] proposed a Multi-Resolution Parallel-Residual Convolutional Neural Network (MPR-CNN) that denoised COVID-19 CXR images by extracting semantic and spatial data through multi-scale features, achieving a Peak Signal-to-Noise Ratio (PSNR) of 38.42 and a Structural Similarity Index Measure (SSIM) of 0.922.

Further, authors in [5] applied preprocessing techniques such as histogram equalization, thresholding, and blurring before classification, achieving 98.31% accuracy on COVID-19 datasets. Authors in [6] introduced a COVID Super-

Resolution-based Siamese Wavelet Multi-Resolution Convolutional Neural Network (COVID-SRWCNN), which enhanced CXRs from low to high resolution, achieving 32.71 PSNR, 92.38 SSIM, and classification accuracy of 99.79%. Similarly, authors in [7] developed a Modified Compact Convolutional Transformer (MCCT) that attained 95.37% accuracy on a four-class CXR dataset, whereas authors in [8] utilized a modified U-Net with a variational encoder for segmentation and ResNet for feature extraction, achieving a PSNR of 43.21 on 2,767 CXR images. Other contributions include [9], where authors proposed a neuromorphic model with alpha- and beta-enhancement preprocessing, achieving PSNR values ranging from 57.37 to 75.15 and classification accuracy of 97.33%. Authors in [10] introduced a Residual-in-Residual (RIR) model with skip connections and dense feature fusion, achieving a PSNR of 39.76 and an SSIM of 94.4. Authors in [11] addressed class imbalance using Deep Convolutional Generative Adversarial Networks (DCGANs), coupled with vision transformer learning, obtaining a PSNR of 33.01, an SSIM of 99.49, and an accuracy of 95.3%. Authors in [12] proposed a Super-Resolution Convolutional Neural Network (SRCNN), achieving PSNR values between 36.38 and 43.28 and SSIM values between 94 and 97.

The existing approaches demonstrate that significant efforts have been made to enhance CXRs for disease classification, employing methods such as multi-resolution Convolutional Neural Networks (CNNs), super-resolution approaches, histogram equalization, and other preprocessing techniques. However, most of these works have primarily focused on improving image quality and resolution for classification, whereas the systematic identification and removal of noise remain underexplored. Addressing this gap, this work introduces a Noise-Aware Convolutional Neural Network (NA-CNN) specifically designed to identify and eliminate noise from CXR images, thereby enhancing image quality and improving classification performance. The main contributions of NA-CNN are as follows:

- Designed and implemented a novel CNN architecture to identify and remove noise from CXR images, thereby improving image quality for subsequent analysis.
- Introduced an innovative method within the CNN to accurately remove various types of noise present in CXR images, including artifacts from patient movement and equipment limitations.
- Conducted extensive experiments on the COVID-19 Radiography dataset to validate the effectiveness of NA-CNN on a diverse set of CXR images, demonstrating significant improvements in image quality.
- Provided a thorough comparative analysis with current existing methods, showcasing superior performance of NA-CNN in terms of noise removal and reduction.

II. METHODOLOGY

When it comes to image processing, CNNs are among the most important methodologies for dealing with and training on enormous datasets. Achieving high-quality images from low-resolution pixels is thus possible with the aid of CNN design. Nevertheless, a limited number of methods currently utilize CNNs to extract high-quality pixels from low-resolution images. In light of the need to further reduce noisy and blurring effects within low-resolution pixels without neglecting necessary quality, this study introduces the NA-CNN architecture, which enables noise elimination in CXR images. Incorporating several unique characteristics into the NA-CNN architecture facilitates rapid computation, accurate implementation, simplified training, and the establishment of a connection between pixels with both high and low resolutions. These unique characteristics allow NA-CNN to be extensively tested for various CXR images and to provide better enhancement results. In the next section the architecture of NA-CNN is discussed.

A. Architecture

The architecture of the NA-CNN is presented in Figure 1, which extracts a highly enhanced quality image from low-resolution-pixels and removes noise. The NA-CNN architecture consists of two phases, i.e., training and testing, where each phase is shown in Figures 2 and 3, respectively.

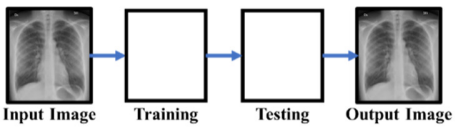

Fig. 1. Architecture of NA-CNN.

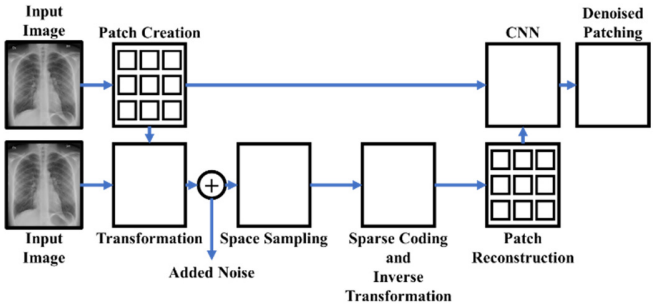

Fig. 2. Training phase of NA-CNN.

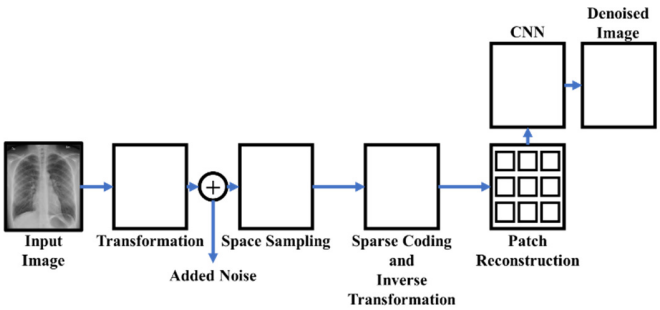

Fig. 3. Testing phase of NA-CNN.

By utilizing structural information, the NA-CNN architecture is able to transform low-resolution pixels into high-resolution pixels. In the training phase, as presented in Figure 2, first, an input image is provided, which is considered to be noisy and of low quality. The image first goes through a

patch-creation process, where patch-wise features are extracted and passed to the NA-CNN layer. Further, the same image is considered, and the patch-wise features are extracted and passed to the transformation layer, where Fourier transform operations are performed for a better understanding of the pixels in two dimensions. Subsequently, noise is added to the input image to enable training on noisy data. In this work, Additive-Gaussian-Noise (AGN) is added to the input image.

The input image then goes through the process of downsampling, where the intermediate pixels are evaluated to increase the visual similarity of low-resolution pixels. Moreover, in the sampling process, each pixel goes through an upsampling process, where it is upsampled to a given size. To achieve an enhanced CXR image, the difference between the sample pixels and downsampled pixels is passed through sparse coding for every pixel. For faster computation, each pixel is processed in parallel and any error caused during parallel processing is handled by spare coding reconstruction. Further, an inverse transformation process takes place using the Fourier Transform to obtain the spatial data.

In the final steps of the training phase, the input image goes through patch recreation, after which it is sent to the NA-CNN layer, where noise is removed, and the trained input image without noise is saved. Similarly, in the testing phase, as presented in Figure 3, the same process is followed as in the training phase, except that the input image is not fed directly to NA-CNN. In the next section, the patch-creation process for extracting images is discussed.

B. Patch Creation for Feature Extraction

As discussed in the architecture, the patches are generated using the input image. This work does not consider any kind of interpolation approach. For creating patches, first, the CXR input image is considered as $\mathbb{X}_D$. The image $\mathbb{X}_D$ is divided into patches and passed to the NA-CNN, where high-quality feature vectors are extracted and convolved utilizing filters. The filters are represented by D_1, L_1, q_1. The first filter, D_1, is set to $D_1 = 5$ for extracting features from the initial image pixels. L_1 is the convolution filter. Three channels are used in the NA-CNN architecture, which are represented using the $YCbCr$ channel; hence, $q_1 = 1$. The first-layer feature extraction for obtaining a high-quality image is represented as $Conv\,(5, m, 1)$ and is further applied over two layers. The process of creating patches is as follows: Consider Z_i, which denotes every column to be a sparse coefficient vector linked with each pixel, and P_j as the objective function for creating patches. The process of patch creation is presented in Algorithm 1.

Algorithm 1: Patch Creation for Feature Extraction
Input: An input CXR image from the COVID-19 dataset i having Z_i
Output: Patch Creation
Step 1: Consider $Z_i = [z_1, z_2, \dots, z_n]$ and $P_j = [p_1, p_2, \dots, p_n]$, where $i = 1,2, \dots, n$ and $j = 1,2, \dots, n$; i is the row vector of Z_i, and j is the column vector of P_j
Step 2: For $j = 1$ to n do
  Create all p_n, $1 \neq j$, and update P_j
  Evaluate minimization function X
  $\min P_j = ||X - p_n Z_i||$ such that $\left|\left|P_j\right|\right|^{2-1}$
  Solve P_j objective function using $P_j = \frac{XZ_j}{\left|\left|XZ_j\right|\right|^2}$
Step 3: End for
Step 4: End

C. Space Sampling

After the patch creation, the transformation takes place, after which noise (AGN) is added. Following this, the space-sampling process takes place where downsampling and upsampling are performed to achieve a high-quality image. From the survey, most existing approaches apply mapping after the feature extraction process and fail to correct the resulting errors. Due to this limitation, they usually end up in extracting high-dimensional features that fail to provide better image quality. This process increases computational overhead and affects the training process. Hence, to solve this issue, downsampling is utilized. To reduce the feature dimensionality n, this work considers downsampling every pixel. This is where the second layer of the NA-CNN architecture comes into place, where D_2 denotes the second-layer filter, which it set to $D_2 = 1$ to achieve better linearity in feature extraction. Further, L_2 is considered as $n \ll m$, where n denotes the parameter for evaluating downsampling. Hence, the second layer of feature extraction is represented as $Conv(1, g, s)$, which reduces feature dimensionality.

Further, the most important stage in our work is adaptive mapping, which helps achieve faster computation. During adaptive mapping, two parameters, width and depth, are used to place filters and layers, respectively. The parameters help in evaluating nonlinear mapping for each high dimensional feature after the downsampling of pixels. Further, adaptive mapping is applied in the third feature extraction layer, where $D_3 = 3$, which represents a medium filter size. To enhance performance, 3×3 layers are considered. In the NA-CNN architecture, a parameter $\mathbb{s}$ is used for determining complexity in computation. In the adaptive mapping layer, every pixel has the same filters; hence, $L_3 = n$. Therefore, the third layer of the NA-CNN architecture is represented as $Conv(3, n, n)$. Moreover, in this mapping layer, the upsampling process is added, which helps in evaluating the difference between the upsampling and downsampling processes, so that it can be sent to sparse-coding reconstruction for every pixel. The down-sampling in the NA-CNN architecture reduces complexity and provides enhanced performance during reconstruction, where upsampling provides a high-quality image for every pixel. To provide synchronization between both sampling approaches, operations are done on 1×1 layers. The upsampling process of the NA-CNN is represented as $Conv(1, m, n)$.

D. Sparse Coding, Inverse Transformation, and Patch Reconstruction

After the process of space sampling, the image goes through sparse-coding reconstruction and inverse transformation. The sparse-coding reconstruction layer is

represented as $SparseCode(9,1,m)$. The difference between both sampling processes helps in sparse-coding reconstruction. The sparse-coding reconstruction process helps reduce errors for every pixel, thus achieving a high-quality image. The inverse transformation is done using the Fourier transform. Further, the patch is reconstructed, following a process similar to patch creation.

E. Noise-Aware Convolutional Neural Network

CNN consists of several layers, each performing specific mathematical operations on the input data to extract features and make predictions. The primary layers in a CNN include the convolutional layer, activation layer, pooling layer, fully connected layer, and output layer. The convolutional layer applies a set of filters (kernels) to the input image to create feature maps. The output feature map Y is represented using the following equation:

$$Y_{i,j,k} = \sum_{m=1}^{M}\sum_{n=1}^{N}\sum_{c=1}^{C}\left[X_{i+m-1,j+n-1,c}\cdot W_{m,n,c,k} + b_k\right] \quad (1)$$

where X is the input image or the input feature map of size $H \times W \times C$, W is the filter (kernel) of size $M \times N \times C \times K$, b_k is the bias term for the k^{th} filter, i and j denote the spatial location in the output feature map, and k denotes the k^{th} filter. H, W, C are the height, width, and number of channels of the input image, respectively, and M, N, K are the height, width, and number of filters, respectively. Instead of using the conventional Rectified Linear Unit (ReLU) for each layer and pixel, this work presents the Noise-Aware (NA) unit. The NA-CNN activation function can be described by the following equation:

$$f(z) = \max(z_k, 0) + \mathbb{B}_k \min(0, z_k) \quad (2)$$

where f represents the activation function, and the input to f is denoted as z_k. $\mathbb{B}_k$ defines the negative-phase coefficient of channel C, where $\mathbb{B}_k$ can be set as 0 or a predefined value. Nevertheless, usually, the $\mathbb{B}_k$ is set to 0. The difference between traditional ReLU and NA-CNN is that NA-CNN discards noise and removes irrelevant features having zero-gradient vectors using the NA unit. The NA unit aids in testing each parameter at multiple levels for every pixel. The sparse coding in the NA-CNN architecture helps define the relationship between input low-resolution pixels and output high-resolution pixels. Due to sparse coding, the output high-resolution image does not have errors and is free of noise. The sparse coding in the NA-CNN architecture to achieve a highly enhanced image is performed using the Modified Learned Iterative Shrinkage and Thresholding (MLIST) approach [13].

The sparse-coding approach is applied to each pixel to achieve better feature representation. The nonlinearity is evaluated using the NA unit. During reconstruction, all pixels in the high-resolution image are used to create a weight map simultaneously. A weight map is generated for each pixel by multiplying the associated pixels. Each product of pixels is then summed to obtain highly enhanced image pixels. This reconstruction process is presented using (3):

$$L(\mathbb{B};\Theta) = \sum_{l}^{q} \mathbb{X}_l(\mathbb{B};\phi_\omega) \odot L_{M_l}(\mathbb{B};\phi_{M_l}) \quad (3)$$

where $\mathbb{B}$ denotes the low-quality input image pixels. Equation (3) has two functions, $\mathbb{X}_l(\mathbb{B};\phi_\omega)$ and $L_{M_l}(\mathbb{B};\phi_{M_l})$, where the first function represents the behavior of the generated weight maps and the second function represents the reconstruction of the high enhanced image pixel M_l. In (3), the multiplication operation is denoted by $\odot$. The loss between the input and output images during training is evaluated using (4):

$$\min_{\Theta} \sum_g \left|\left|L(\mathbb{B}_g;\Theta) - b_g\right|\right|_2^2 \quad (4)$$

In (4), $L(\mathbb{B}_g;\Theta)$ represents the output image pixels, $\mathbb{B}_g$ represents the highly enhanced image, Θ represents the group of parameters, and b_g represents the low-quality image pixels. The performance of NA-CNN is evaluated in the next section and compared with existing approaches.

III. RESULTS AND DISCUSSION

A. System Requirements, Dataset and Performance Metrics

The evaluation was conducted on an Intel Core i7 processor, integrated with NVIDIA GeForce GTX GPU, along with 16 GB of RAM. Evaluations were performed using MATLAB. The evaluations were performed in terms of PSNR and SSIM, as all the existing works have used similar metrics. PSNR helps in evaluating the restored image quality by comparing the input and output images. A higher PSNR indicates better reconstruction, i.e., a higher-quality image. PSNR is evaluated using (5), where MSE represents the Mean Squared Error.

$$\text{PSNR} = \frac{10\log_{10}(L-1)^2}{\text{MSE}} \quad (5)$$

Further, SSIM helps in evaluating similarities between input and output images. To quantify the reduction in image quality while preserving structural information, SSIM is used. SSIM is evaluated using (6), where μ_1 and μ_2 represent the mean intensities of the input and output images, respectively. Parameters σ_1 and σ_2 represent the variances of the input and output images, respectively, σ_{12} denotes the covariance between the input and output images, and U_1 and U_2 denote constants used to stabilize weak pixel values.

$$\text{SSIM}(x_1, x_2) = \frac{(2\mu_1\mu_2+U_1)(2\sigma_{12}+U_2)}{(\mu_1+\mu_2+U_1)(\sigma_1+\sigma_2+U_2)} \quad (6)$$

B. Performance Evaluation

For the evaluation, this work considered the dataset provided in [14], which has four classes, i.e., COVID-19, Lung Opacity, Normal, and Pneumonia. For the collection of this dataset, a collaborative research team from the Qatar University, Doha, Qatar, and the University of Dhaka, Bangladesh, together with collaborators from Pakistan and Malaysia, and in close cooperation with medical professionals, developed a comprehensive CXR dataset known as the "COVID-19 Radiography Database" [15, 16]. The dataset was released in multiple stages. The initial release included 219 COVID-19, 1,341 Normal, and 1,345 Viral Pneumonia CXR images. In the first update, the number of COVID-19 images was expanded to 1,200. The second update further enriched the dataset, increasing it to 3,616 COVID-19, 10,192 Normal, 6,012 Lung Opacity (non-COVID lung infection), and 1,345

Viral Pneumonia images, along with corresponding lung segmentation masks. This dataset was selected for evaluation in this study because several existing approaches, including [4] and [11], have also employed the same dataset, thereby facilitating a fair and direct comparative analysis. The results for the different classes are presented in Figures 4, 5, 6, and 7 for COVID-19, Lung Opacity, Pneumonia, and Normal, respectively.

(a) (b) (c)

Fig. 4. Preprocessing of COVID-19 image: (a) COVID-19 input image, (b) noise-induced input image, (c) preprocessed image using NA-CNN.

(a) (b) (c)

Fig. 5. Preprocessing of Lung Opacity image: (a) Lung Opacity input image, (b) noise-induced input image, (c) preprocessed image using NA-CNN.

(a) (b) (c)

Fig. 6. Preprocessing of Pneumonia image: (a) Pneumonia input image, (b) noise-induced input image, (c) preprocessed image using NA-CNN.

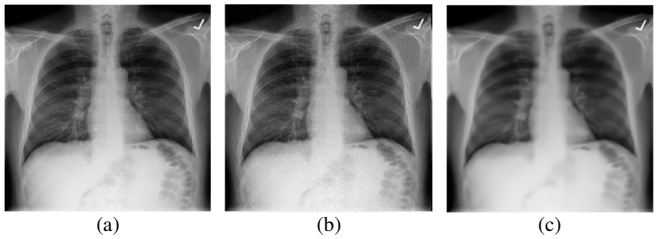

(a) (b) (c)

Fig. 7. Preprocessing of Normal image: (a) Normal input image, (b) noise-induced input image, (c) preprocessed image using NA-CNN.

The PSNR and SSIM achieved by the NA-CNN are compared with those of the MPR-CNN [4]. Figures 8 and 9 illustrate the performance of both models across different noise levels. At a noise level of 15, MPR-CNN achieved a PSNR of 38.48 and an SSIM of 0.922, whereas NA-CNN performed slightly better, with a PSNR of 39.84 and an SSIM of 0.937. This indicates that NA-CNN produces higher-quality images with less distortion and better structural similarity to the original images compared to MPR-CNN at this noise level. When the noise level increased to 25, MPR-CNN's performance decreased, yielding a PSNR of 36.88 and an SSIM of 0.900. NA-CNN, however, maintained better performance, with a PSNR of 37.84 and an SSIM of 0.912. This further illustrates NA-CNN's robustness in handling higher noise levels while still delivering higher-quality reconstructions than MPR-CNN.

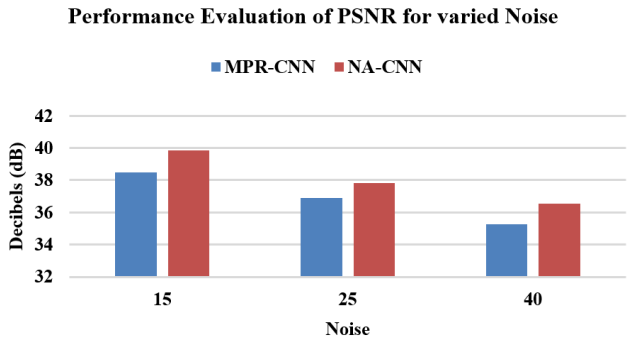

Fig. 8. PSNR performance evaluation.

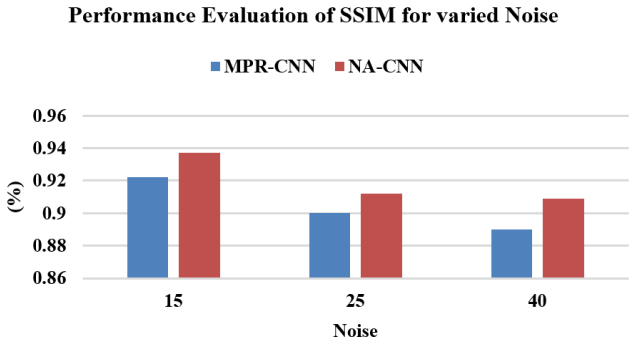

Fig. 9. SSIM performance evaluation.

At the highest noise level of 40, both models experienced a drop in performance, but NA-CNN continued to outperform MPR-CNN. MPR-CNN achieved a PSNR of 35.28 and an SSIM of 0.890, whereas NA-CNN attained a PSNR of 36.54 and an SSIM of 0.909. Despite the increased noise, NA-CNN consistently provided better image quality and structural fidelity compared to MPR-CNN across all tested noise levels. Overall, NA-CNN demonstrates superior performance over MPR-CNN in terms of both PSNR and SSIM at varying noise levels, indicating its effectiveness in producing higher-quality images and better preserving the structural integrity of the original images under noisy conditions.

C. Comparative Study

Table I presents a comparative analysis of different image enhancement models based on PSNR and SSIM, which are widely used to evaluate reconstruction quality and structural fidelity. The MPR-CNN model [4], evaluated on the COVID-19 Radiography Database [14], achieved a PSNR of 36.88 and an SSIM of 0.922, indicating satisfactory image quality and structural preservation. In contrast, the DCGAN with Compact Convolutional Transformer (CCT) model [11] reported a lower

PSNR of 33.01, but achieved an exceptionally high SSIM of 0.9949, demonstrating its strong ability to preserve structural information despite reduced pixel-level accuracy on the same dataset [14]. The proposed NA-CNN model outperformed the existing methods by achieving the highest PSNR of 39.84, along with a competitive SSIM of 0.937, on the COVID-19 Radiography Database [14]. These results indicate that NA-CNN provides superior noise removal and reconstruction quality while effectively preserving structural details. Overall, NA-CNN demonstrates the best balance between image quality and structural similarity, highlighting its robustness and efficiency for medical image enhancement tasks.

TABLE I. COMPARATIVE STUDY

Ref, year	Model	PSNR	SSIM
[4], 2021	MPR-CNN	36.88	0.922
[11], 2024	DCGAN+CCT	33.01	0.9949
Proposed	NA-CNN	39.84	0.937

IV. CONCLUSION

This work presents the Noise-Aware Convolutional Neural Network (NA-CNN) approach, a novel method for enhancing low-resolution medical images, specifically Chest X-Rays (CXRs), by effectively eliminating noise and improving image quality. By leveraging Convolutional Neural Networks (CNNs) combined with sparse coding reconstruction, the NA-CNN model achieved superior performance compared to existing methods. The proposed work introduces innovative techniques such as adaptive downsampling, nonlinear mapping, and an improved activation function, which collectively contribute to its robustness and efficiency. The evaluation results, conducted on a high-performance system with an extensive dataset, demonstrated that NA-CNN consistently outperforms the MPR-CNN model across various noise levels, achieving higher Peak Signal-to-Noise-Ratio (PSNR) and Structural Similarity Index Measure (SSIM) values. With a PSNR of 39.84 and an SSIM of 0.937, NA-CNN surpassed other models such as the Multi-Resolution Parallel-Residual Convolutional Neural Network (MPR-CNN) and the Deep Convolutional Generative Adversarial Network with Compact Convolutional Transformer (DCGAN)+CCT, which, although effective in certain aspects, do not match the overall performance of NA-CNN. The NA-CNN model represents a significant advancement in the field of medical image processing, providing a robust and efficient solution for transforming low-resolution images into high-resolution counterparts. Its ability to handle large datasets with low computational complexity and high processing speed makes it an invaluable tool for medical professionals. Future work could explore further optimization and real-world deployment of the NA-CNN model, potentially extending its application to other types of medical images and enhancing its capabilities through continuous learning and adaptation. Additionally, the NA-CNN model can be extended for segmenting CXR images, further broadening its clinical utility.

REFERENCES

[1] G. S. Gould *et al.*, "Recognising the importance of chronic lung disease: a consensus statement from the Global Alliance for Chronic Diseases (Lung Diseases group)," *Respiratory Research*, vol. 24, no. 1, Jan. 2023, Art. no. 15, https://doi.org/10.1186/s12931-022-02297-y.

[2] G. Rasool *et al.*, "COVID-19: A threat to the respiratory system," *International Journal of Immunopathology and Pharmacology*, vol. 38, Aug. 2024, Art. no. 03946320241310307, https://doi.org/10.1177/03946320241310307.

[3] N. C. Kundur, B. C. Anil, P. M. Dhulavvagol, R. Ganiger, and B. Ramadoss, "Pneumonia Detection in Chest X-Rays using Transfer Learning and TPUs," *Engineering, Technology & Applied Science Research*, vol. 13, no. 5, pp. 11878–11883, Oct. 2023, https://doi.org/10.48084/etasr.6335.

[4] X. Jiang, Y. Zhu, B. Zheng, and D. Yang, "Images denoising for COVID-19 chest X-ray based on multi-resolution parallel residual CNN," *Machine Vision and Applications*, vol. 32, no. 4, June 2021, Art. no. 100, https://doi.org/10.1007/s00138-021-01224-3.

[5] A. Giełczyk, A. Marciniak, M. Tarczewska, and Z. Lutowski, "Pre-processing methods in chest X-ray image classification," *Plos One*, vol. 17, no. 4, Apr. 2022, Art. no. e0265949, https://doi.org/10.1371/journal.pone.0265949.

[6] H. N. Monday *et al.*, "COVID-19 Diagnosis from Chest X-ray Images Using a Robust Multi-Resolution Analysis Siamese Neural Network with Super-Resolution Convolutional Neural Network," *Diagnostics*, vol. 12, no. 3, Mar. 2022, Art. no. 741, https://doi.org/10.3390/diagnostics12030741.

[7] I. U. Khan *et al.*, "An effective approach to address processing time and computational complexity employing modified CCT for lung disease classification," *Intelligent Systems with Applications*, vol. 16, Nov. 2022, Art. no. 200147, https://doi.org/10.1016/j.iswa.2022.200147.

[8] H. Sun *et al.*, "Artificial intelligence-assisted multistrategy image enhancement of chest X-rays for COVID-19 classification," *Quantitative Imaging in Medicine and Surgery*, vol. 13, no. 1, pp. 39416–39416, Jan. 2023, https://doi.org/10.21037/qims-22-610.

[9] J. S. Jennifer and T. S. Sharmila, "A Neutrosophic Set Approach on Chest X-rays for Automatic Lung Infection Detection," *Information Technology and Control*, vol. 52, no. 1, pp. 37–52, Mar. 2023, https://doi.org/10.5755/j01.itc.52.1.31520.

[10] A. Khishigdelger, A. Salem, and H.-S. Kang, "Elevating Chest X-ray Image Super-Resolution with Residual Network Enhancement," *Journal of Imaging*, vol. 10, no. 3, Mar. 2024, Art. no. 64, https://doi.org/10.3390/jimaging10030064.

[11] Md. Z. Hasan *et al.*, "Fast and Efficient Lung Abnormality Identification With Explainable AI: A Comprehensive Framework for Chest CT Scan and X-Ray Images," *IEEE Access*, vol. 12, pp. 31117–31135, 2024, https://doi.org/10.1109/ACCESS.2024.3369900.

[12] S. Rani and N. Kaur, "Medical X-ray images enhancement based on super resolution convolution neural network," *International Journal of Informatics and Communication Technology*, vol. 13, no. 2, pp. 257–263, Aug. 2024, https://doi.org/10.11591/ijict.v13i2.pp257-263.

[13] J. C. Hauffen, L. Kästner, S. Ahmadi, P. Jung, G. Caire, and M. Ziegler, "Learned Block Iterative Shrinkage Thresholding Algorithm for Photothermal Super Resolution Imaging," *Sensors*, vol. 22, no. 15, July 2022, Art. no. 5533, https://doi.org/10.3390/s22155533.

[14] "COVID-19 Radiography Database." Kaggle. [Online]. Available: https://www.kaggle.com/datasets/tawsifurrahman/covid19-radiography-database.

[15] M. E. H. Chowdhury *et al.*, "Can AI Help in Screening Viral and COVID-19 Pneumonia?," *IEEE Access*, vol. 8, pp. 132665–132676, 2020, https://doi.org/10.1109/ACCESS.2020.3010287.

[16] T. Rahman *et al.*, "Exploring the effect of image enhancement techniques on COVID-19 detection using chest X-ray images," *Computers in Biology and Medicine*, vol. 132, May 2021, Art. no. 104319, https://doi.org/10.1016/j.compbiomed.2021.104319.